You Know The Temperature at the Weather Station But Do You Know It Anywhere Else? Assessing Land Surface Temperature Using Landsat ETM+ Data

J. R. Otukei, T. Blaschke

Abstract

Land Surface Temperature (LST) is one of the important parameters affecting climate change. This study investigated the potential of Landsat ETM+ low and high Thermal InfraRed (TIR) bands for assessing the LST in Kampala, Mukono and Jinja Districts. Data analysis was carried out using the Apparent Reflectance (AR) and FLAASH models. The LST estimates derived from the TIR bands was validated using available ground truth data. The analysis of low gain TIR band using the AR model provided the lowest error of 0.71^{o}C. Furthermore, areas with high green vegetation cover were found to have low LST and high emissivity values. In Contrast, bare ground and urban areas had low emissivity and high LST. Overall, Landsat ETM+ TIR bands provide a high potential for assessing LST at local scales. The results obtained are not only of high accuracy but also provides spatial distribution of LST at local scales, which is not possible with traditional methods.

Keywords: Landsat ETM+, Land Surface Temperature, Apparent Reflectance and FLAASH Models

1. Introduction

Remote sensing of Land Surface Temperature (LST) has become an important research area in past decades (Jimenez-Munoz, Sobrino et al. 2003; Qin, Zhang et al. 2011; Sobrino, Jimenez-Munoz et al. 2004; Valor and Caselles 1996). This can be attributed to the diverse applications of the LST parameter, for example, weather prediction, geothermal area detection, monitoring urban heat evolution, detection of land use and land cover change, global ocean circulation, climatic change analysis and analysis of energy and matter exchanges between atmosphere and surfaces (Qin, Zhang et al. 2011; Valor and Caselles 1996). Furthermore, the limitation of traditional *insitu* measurements which are carried out in a few selected weather station points necessitates new approaches for LST measurement. Data from satellite sensors such as the Moderate Resolution Imaging Spectrometer (MODIS), Advanced Spaceborne Thermal Emission Reflection Radiometer (ASTER), the National Oceanic and Atmospheric Administration- Advanced Vey High Resolution Radiometer from (NOAA-AVHRR), Landsat ETM/ETM+ and Meteosat Second Generation/Spinning Enhanced Visible and Infrared Imager (MSG-SEVIRI) have become attractive options for LST estimation.

While advances have been made in LST estimation from satellite data, there are still some challenges that affect the accuracy of the derived LST values. For example, the satellite systems measure the upwelling thermal radiation which is used as a proxy for estimating the LST. Unfortunately, the measured radiation is affected by atmospheric constituents before reaching the sensors resulting in inaccurate LST estimates. Moreover, the thermal radiation is detected in only one direction. Whereas it is possible to make atmospheric corrections for the observed radiation, an additional critical problem in the estimation of LST from remote sensing data is the separation of coupled temperature and emissivity parameters (Sobrino, Jimenez-Munoz et al. 2002). As a result, given a sensor of N channels, there will be only N observations but N+1 unknowns, that is, the N emissivity measurements and 1 temperature measurement (Valor and Caselles 1996). This makes it difficult to separate temperature from emissivity using passive radiometry since the system of equations has no unique solution. Several approaches have been developed to handle the N+1 unknown parameter problem. Among these are the single or multi-channel (split window) and dual angle approaches (Jimenez-Munoz, Sobrino et al. 2003; Liang 2001; Valor and Caselles 1996). The main aim of this study was to provide the LST estimates using Landsat ETM+ satellite data. The Landsat ETM+ was preferred due to its high spatial resolution, which is essential for LST analysis at large scales.

2. Theoretical basis for land surface temperature measurement

The theoretical basis for the LST measurement is the Plank's radiation function formulated as:

$$B(\lambda,T) = \frac{C_1\lambda^{-5}}{\pi\left[e^{\left(\frac{C_2}{\lambda T}\right)}-1\right]} \qquad (1)$$

Where: $B(\lambda,T)$ is the spectral radiance of a blackbody ($WM^{-2}sr^{-1}\mu m^{-1}$) and independent terms are the wavelength (λ) in meters, temperature (T) in degree Kelvin, the first radiation constant C1=3.741775x10^{-22} Wm^2, and the second radiation constant C2 = 1.4388 x 10^{-2}mK and PI (π) = 3.14. In order to calculate the radiance that corresponds to the brightness temperature within the given band, equation 1 is integrated over an instrument response function resulting in equation 2 (Alley and Nilsen 2001).

$$B(\lambda,T)_s = \frac{\int \psi(\lambda)B(\lambda,T)(T,\lambda)d\lambda}{\int \psi(\lambda)d\lambda} \qquad (2)$$

Where: $B(\lambda,T)_s$is the radiance recorded at the sensor and ψ is the instrument function. The determination of the value of T as a function of $B(\lambda,T)_s$ can then be achieved through the inversion of equation 1. It is however, known that inversion of equation 2 cannot be done explicitly and consequently, only approximate solutions can be obtained (Alley and Nilsen 2001). The most commonly used and straight forward method is that obtained by replacing the response function with a delta function, resulting in equation of the form:

$$T = \frac{C_2}{\lambda ln\left[\left(\frac{C_1}{\pi\lambda^5 B(\lambda,T)}+1\right)\right]} \quad (3)$$

Although the value of T gives the temperature at the top of the atmosphere, it does not represent the real surface (land or sea) temperature. Specific algorithms are therefore necessary to convert the value of T to LST. A well-known algorithm for this purpose is that based on the split-window method (Mao, Qin et al. 2005; Zhang, He et al. 2006). Unfortunately, the split-window algorithm cannot be applied for the analysis of Landsat ETM+ data since it requires more than two thermal bands. In this regard, approaches based on single channels were adopted for the analysis.

3. Materials and methods

3.1Study area

The study area is shown in Figure 1 and is located between latitudes ($0^0$41'-$0^0$31') N and longitudes ($32^0$00'-$33^0$19') E. It covers the urban landscapes of Kampala, Jinja, Entebbe, Mukono, and their surrounding areas. A part from Mabira forest which is easily identifiable in the false colour composite image shown in Figure 1, most of the other vegetation categories can be generally classified as mixed. There are also some commercial tea and sugar plantations located in Mukono and Jinja areas. Included in the study area are parts of Lake Victoria and the source of River Nile.

3.2 Data

An orthorectified Landsat ETM+ data located on satellite path 171 and row 060, acquired on February 10, 2006 was used for the investigation. Since the satellite image was collected after the malfunctioning of the scan line corrector (SLC-off), it has inherent ziz-zag lines towards the right and left edges of the image. While it is possible to correct for the observed phenomena, such an operation was not necessary in this case since the study area falls in the middle of the scene where there is no noticeable image distortion.

3.3 Data pre-processing for temperature retrieval

The conceptual framework used in this study for LST retrieval from Landsat ETM+ data follows that proposed by Qin et al. (2011). It requires radiometric calibration, atmospheric correction and emissivity estimation, prior to LST estimation.

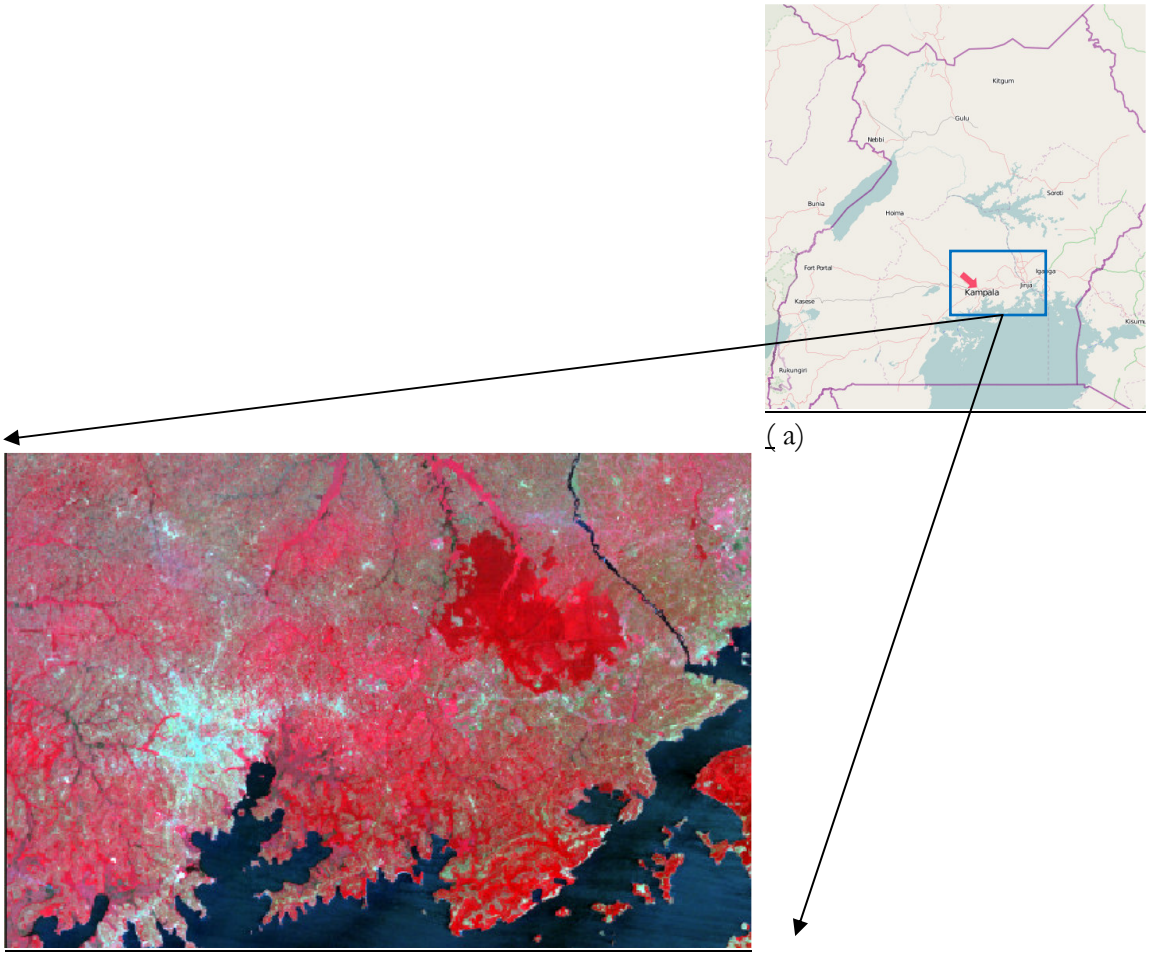

Figure 1: Study area. The map of Uganda (a) was obtained from the http://www.openstreetmap.org/ website while the Landsat ETM+ data whose false colour composite is shown in (b) was accessed from the Land Cover facility website http://glcf.umiacs.umd.edu/

3.3.1 Radiometric calibration

Radiometric calibration was performed by converting the Digital Number (DN) values to radiance based on sensor calibration parameters. This operation was accomplished using equation 4:

$$L_\lambda = \left(\frac{LMAX_\lambda - LMIN_\lambda}{QCALMAX - QCALMIN}\right) * (QCAL - QCALMIN) + LMIN_\lambda \quad (4)$$

Where: L_λ is the spectral radiance at the sensors aperture and the terms on the right hand of the equation are the spectral radiances scaled to QCALMAX ($LMAX_\lambda$) and QCALMIN ($LMIN_\lambda$), the minimum and maximum quantised calibrated pixel values ($QCALMIN$) and ($QCALMAX$), corresponding to$LMIN_\lambda$ and $LMAX_\lambda$ and the quantised calibrated pixel value (QCAL). Radiometric calibration was applied to both multispectral and thermal bands of Landsat ETM+ data.

3.3.2 Atmospheric correction

The DN values recorded at given pixel locations by a satellite sensor are not always true radiance values due to a number of factors. Among these are the effects of atmospheric scattering and absorption, environment radiance which produces the adjacency effect, variation of illumination geometry including the Sun's azimuth and zenith angles, ground slope and deposition of the topographic objects (Mather 2004). Therefore, minimisation of the effects caused by atmospheric conditions as well as the variation in illumination geometric is a pre-requisite for successful derivation of parameters of interest from remote sensing data. Atmospheric effects are generally less pronounced with the long wavelength radiations compared to short wave radiation. Accordingly, the visible bands of Landsat ETM+ are more affected by atmospheric varying atmospheric conditions than the infrared and mid-infrared bands. Pre-processing of the multispectral bands was therefore necessary to make corrections for the atmospheric and solar illumination effects.

Whereas there are different methods used for atmospheric correction (Lu, Mausel et al. 2002), only approaches that do not require ground truth or in situ data were preferred for this study. This is because the physical-based models such as the second simulation of satellite signal in solar spectrum (6S), moderate resolution atmospheric radiance and transmittance model (MODTRAN) and LOWTRAN, although recognised as more accurate methods, require ground truth or in situ data. Moreover, collecting ground truth data for an archived Landsat ETM+ data is unrealistic. Image based models on the other hand do not require in situ data since the only input parameters are the images and some header file for extracting information such as the acquisition date, sun elevation angle, gain and bias. An apparent reflectance (AR) model (Gebreslasie, Ahmed et al. 2009) and FLAASH model were selected for atmospheric correction. The AR is rather simple approach which corrects the effects of variation of solar radiation and sun zenith based on equation 5.

$$\rho_\lambda = \left(\frac{\pi * L_\lambda * d^2}{ESUN * \cos(\theta)}\right) \qquad (5)$$

Where ρ_λ is the reflectance, and the independent terms are the radiance (L_λ), the earth-sun distance (d) measured in astronomical units, the mean or exo-atmospheric solar irradiance (ESUN) in a given band in units of $mWcm^{-2}\mu m^{-1}$and solar zenith angle (θ) measured in radians. It is important to note that the AR model shown in equation 5 does not account for atmospheric scattering and absorption. Perhaps this is the main limitation of the model.

The FLAASH algorithm on the other hand is rather complex and robust and based on the MODTRAN4 atmospheric correction algorithm (Adler-Golden, Matthew et al. 1999). Unlike the AR model, additional sensor specific parameters have to be specified for implementation of the FLAASH model. Some of the parameters such as the aerosol and atmospheric model that require some knowledge of the study area were not considered in the analysis process.

3.3.3 Estimation of emissivity

Due to the coupling between the emissivity and temperature, knowledge of emissivity is important for LST estimation. But, the estimation of emissivity is known to be a complex task. Two of the common approaches used for emissivity estimation are the Look-Up-Table (LUT) and Fraction Vegetation Cover (FVC). The LUT approach requires a priori image classification and thereafter applying the LUT to assign the emissivity of the known cover types to the resultant classes. This approach is possible if the area of study can be classified into classes of known emissivity values. The complexities of the different land cover classes in different regions make it impossible to classify the image into the standard land cover classes of known emissivities. Additionally, handling block membership on fragmented land cover types is still a challenging task. An alternative approach is to estimate the emissivities using the FVC computed from the normalised vegetation index (NDVI). Since the FVC facilitates the derivation of the emissivities from the image, it was preferred in this study than the LUT approach. The FVC estimates were computed on the basis of equation 6:

$$FVC = \left[\frac{NDVI - NDVI_{min}}{NDVI_{max} - NDVI_{min}}\right]^2 \quad (6)$$

Where the independent terms are: the Normalised Difference Vegetation Index (NDVI) for each pixel and the maximum and minimum set thresholds of the pure pixels $NDVI_{max}$ and $NDVI_{min}$ respectively. For this study the thresholds for the pure soil and vegetation pixels were taken as 0.2 and 0.5 respectively, based on similar existing studies (Sobrino, Jimenez-Munoz et al. 2004). The NDVI values were computed using the atmospheric corrected reflectance values. All the pixels whose NDVI values were less than the $NDVI_{min}$ were assigned the emissivity value of 0.97. This value corresponds to the emissivity of pure soils. On the other hand, the pixels with NDVI value greater than $NDVI_{max}$ were assigned the emissivity value of 0.99, corresponding to the emissivity of pure vegetation. The emissivities of pure ground and vegetation pixels and were also obtained from the literature. The emissivities of the remaining mixed pixels were estimated using equation 7:

$$\varepsilon = \varepsilon_v(FVC) + \varepsilon_{sg}(1 - FVC) + d\varepsilon \quad (7)$$

Where: ε_v and ε_g are the emissivities of the pure vegetation and ground pixels, FVC, is the fractional vegetation cover and $d\varepsilon$ is the error term defined using equation 8. The value of F was taken to be 0.55 and represents an average shape factor for different geometrical distributions.

$$d\varepsilon = (1 - \varepsilon_s)(1 - FVC_v)F\varepsilon_v \quad (8)$$

3.4 Derivation of land surface temperature from Landsat ETM+ thermal band

Equation 9, which is a simplified form of equation 1, was used to compute the at-sensor-brightness temperature T_s (K), where K_1 and K_2 are constants whose values are 1282.7108 (K) and 666.093 ($Wm^{-2}sr^{-1}\mu m^{-1}$) respectively and L_s is the at-sensor-radiance. The resulting brightness temperature was converted to the land surface temperature (LST) using equation 10, where λ is wavelength of the emitted radiance

whose value is 11.5µm for the case of Landsat ETM+, ε is the emissivity derived using equation 7. The parameter ρ is the constant defined using equation 11 whose independent terms are planks constant (h), speed of light (c) and Boltzmann constant (δ). The values of h, c and δ are: $6.26\text{x}10^{-34}$Js, $3.0\text{x}10^{8}$m/s and $1.38\text{x}10^{-23}$J/K respectively. The final derived LST, initially in Kelvin was converted to degree centigrade.

$$T_s = \frac{K_2}{\ln\left(1+\frac{K_1}{L_s}\right)} \quad (9)$$

$$LST = \frac{T_S}{1+\left(\lambda\times\frac{T_S}{\rho}\right)\ln\varepsilon} \quad (10)$$

$$\rho = \frac{h\times c}{\delta} \quad (11)$$

Validation of the resulting estimated LST was performed using available ground truth data. Unfortunately, only a single LST value for the Entebbe airport was available for testing. This included recorded hourly LST measurements taken on the day the satellite date was acquired. Since the Landsat data was acquired at 10.51 am, the corresponding temperature was estimated using linear interpolation based on the station measurements at 10.00 am and 11.00 am. The resulting estimate was used for validating the LST estimated from the Landsat ETM+ TIR bands.

4. Results and discussion

Figures 2 and 3 show the spatial distribution of surface emissivity and LST respectively in the selected study area. Both the low and high gain Landsat ETM+TIR bands were used for the investigation. Corresponding summary statistics of the resulting temperature estimates derived using the AR and FLAASH models are provided in Table 1. Table 2 on the other hand shows ground truth temperatures at the test site taken at 10.00 am and 11.00 a.m, as well as the estimated ground truth temperature during the satellite path at 10.51 am. The ground truth estimate was subtracted from the temperature estimates from Landsat ETM+ TIR bands and the resulting errors are provided in Table 1. The lowest error of 0.71^{o}C was obtained using the low gain thermal band, analysed using the AR model. For this case, the temperature range was between (21.21-67.17)^{o}C with a mean and standard deviations of 29.51^{o}C and 3.625^{o}C respectively. These results show LST variation. Overall, areas with high vegetation cover such as the Mabira forest showed low temperature estimates while areas with low vegetation cover including the built up areas of Kampala had high temperature estimates. High temperature values were also observed in the Northern and Eastern parts of the study area. Preliminary investigation using Google Maps and Landsat ETM+ showed that those areas were either bare ground or cleared sugar plantations areas. These observations are similar to those provided by Mallick et al. (2008) who estimated the LST over Delhi using Landsat ETM+ data. Results also showed the dependency of surface temperature on emissivity. Highly green vegetated areas with high emissivity such as the Mabira forest had low LST estimates. In contrast urban areas such as Kampala had low emissivities but with high observed LST values.

Olioso et al. (2007) carried out a study to investigate the low thermal surface temperature emissions in presence of dry vegetation. The results showed a strong correlation between NDVI with temperature in such a way that areas with high NDVI also had a high emissivity. Since NDVI is related with high vegetation cover, the results obtained in this study are therefore comparable to those obtained in early studies. On the validation results, while data from a single test site was available, an additional challenge of validating surface temperature derived from Landsat data is the dissimilarity of the spatial scales between Landsat data estimates and field measurements. This becomes critical especially when the terrain is heterogeneous. Despite these observations, it can still be argued that the estimates obtained from the study agree with the ground truth data. In all the cases investigated, the magnitude of error in the surface temperature estimate was less than 2^{o}C which is comparable to the results in the literature (Srivastava, Majumdar et al. 2009).

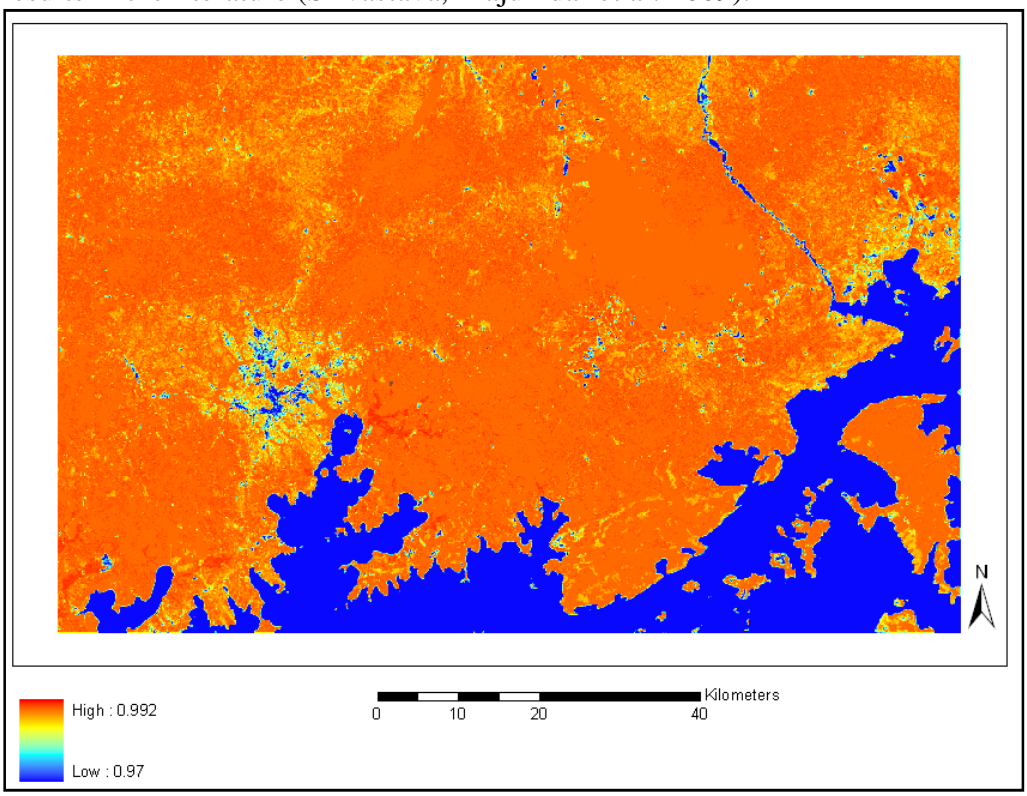

Figure 2:Emissivity distribution

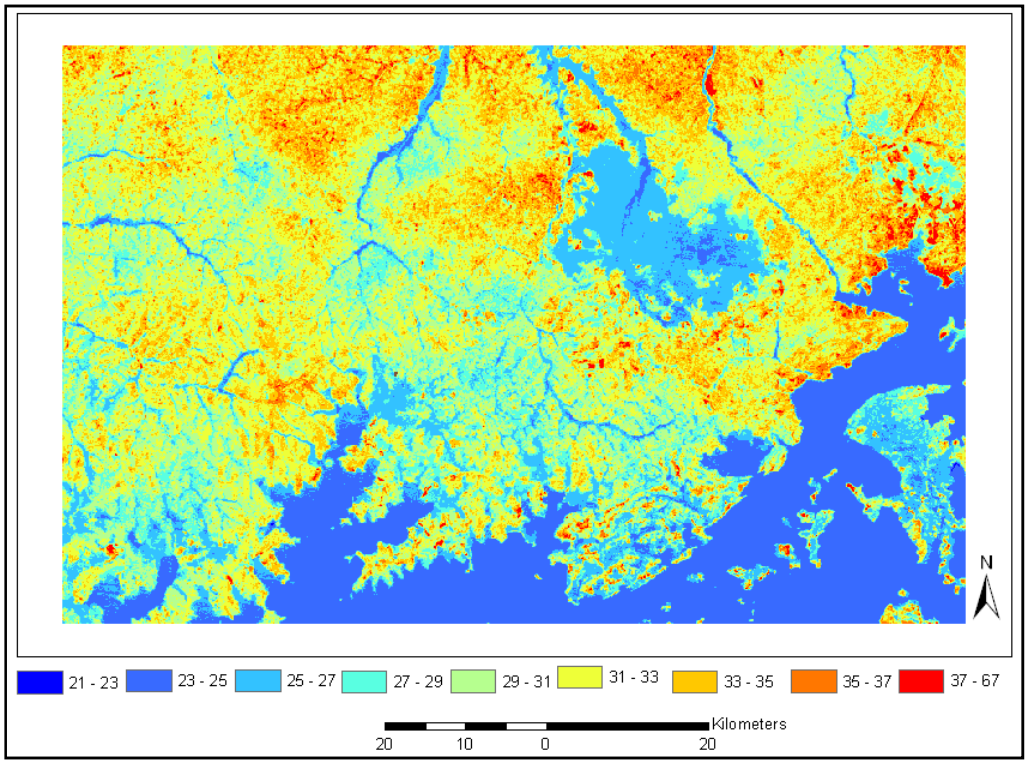

Figure 3:Land surface temperature distribution

Table 1. Summary statistics obtained using the AR and FLAASH models

Parameter	TM61-AR	TM62-AR	TM61- FLAASH	TM62-FLAASH
Minimum	21.21	21.08	21.21	21.08
Maximum	67.17	51.47	67.17	51.48
Mean	29.51	29.42	29.49	29.39
Standard	3.625	3.61	3.59	3.58
Test	28.14	27.95	27.34	27.25
Error	-0.71	-0.90	-1.51	-1.60

Table 2. Validation data at Entebbe weather station (0.1N, 32.5E)

Time	Temperature (degrees)
10.00 am	28
10.51 am	28.85
11.00 am	29

5. Conclusion and recommendations

The results of the investigation show an agreement of the LST derived from Landsat ETM+ TIR bands with the ground truth data. The low gain TIR band provided the best estimate with an error of less than 1^{o}C. All other approaches resulted in errors of magnitude of less than 2^{o}C. This error is acceptable taking into consideration the differences in spatial scales between ground measurements and estimates from Landsat

ETM TIR bands. Based on the results of this study as well as those in the literature, it can be concluded that Landsat ETM+ data provides a high potential for surface temperature estimation. However, there is need for further research to investigate the effect of the different land cover and land use patterns on surface temperature in Uganda. Such studies will contribute towards climate change which is one of the global challenges affecting mankind.

Acknowledgment

The author thanks the Global Land Cover Facility (GLCF) for providing the Landsat data and NASA for the atmospheric correction parameters.

References

Adler-Golden, S. M., M. W. Matthew, et al. (1999). Atmospheric Correction for Short-wave Spectral Imagery Based on MODTRAN4. SPIE Proceeding, imaging spectrometry V, Society of Photo-Optical Instrumentation Engineers.

Alley, R. E. and M. J. Nilsen (2001). Algorithm Theoretical Basis Document for Brightness Temperature: Version 3.1. Pasadena, California, Jet Propulsion Laboratory.

Gebreslasie, M. T., F. B. Ahmed, et al. (2009). "Image-based reflectance conversion of ASTER and IKONOS imagery as precursor to structural assessment of plantation forests in KwaZulu-Natal, South Africa." Southern Forest**71**(4): 259-265.

Jimenez-Munoz, J. C., J. A. Sobrino, et al. (2003). "Synergistic use of DAIS bands to retrieve land surface emissivity and temperature." Igarss 2003: IEEE International Geoscience and Remote Sensing Symposium, Vols I - Vii, Proceedings: 1062-1064.

Liang, S. L. (2001). "An optimization algorithm for separating land surface temperature and emissivity from multispectral thermal infrared imagery." IEEE Transactions on Geoscience and Remote Sensing**39**(2): 264-274.

Lu, D., P. Mausel, et al. (2002). "Assessment of atmospheric correction methods for Landsat TM data applicable to Amazon basin LBA research." International Journal of Remote Sensing**23**(13): 2651-2671.

Mallick, J., Y. Kant, et al. (2008). "Estimation of land surface temperature over Delhi using Landsat-7 ETM+." J.Ind.Geophys. Union**12(3)**: 131-140.

Mao, K., Z. Qin, et al. (2005). "A practical split-window algorithm for retrieving land-surface temperature from MODIS data." International Journal of Remote Sensing**26**(15): 3181-3204.

Mather, P. M. (2004). Computer processing of remotely sensed images: An Introduction, 3rd Edition. West Sussex, England, John Willey and Sons.

Olioso, A., G. Sòria, et al. (2007). "Evidence of Low Land Surface Thermal Infrared Emissivity in the Presence of Dry Vegetation." IEEE Geoscience and Remote Sensing Letters**4 (1)**.

Qin, Q., N. Zhang, et al. (2011). "Geothermal area detection using Landsat ETM+ thermal infrared data and its mechanistic analysis—A case study in Tengchong, China." International Journal of Applied Earth Observation and GeoInformation**13**: 552-559.

Sobrino, J. A., J. C. Jimenez-Munoz, et al. (2004). "Single-channel and two-channel methods for land surface temperature retrieval from DAIS data and its application to the Barrax site." International Journal of Remote Sensing**25**(1): 215-230.

Sobrino, J. A., J. C. Jimenez-Munoz, et al. (2002). "Surface emissivity retrieval from Digital Airborne Imaging Spectrometer data." Journal of Geophysical Research-Atmospheres**107**(D23): -.

Srivastava, P. K., T. J. Majumdar, et al. (2009). "Surface temperature estimation in Singhbhum Shear Zone of India using Landsat-7 ETM+ thermal infrared data." Advances in Space Research**43**: 1563-1574.

Valor, E. and V. Caselles (1996). "Mapping land surface emissivity from NDVI: Application to European, African, and South American areas." Remote Sensing of Environment**57**(3): 167-184.

Zhang, Z. M., G. J. He, et al. (2006). "Land Surface Temperature Retrieval of Beijing city using MODIS and TM Data." 2006 IEEE International Geoscience and Remote Sensing Symposium, Vols 1-8: 1094-1096.